

Modeling of thin film bulk acoustic wave resonators and ladder-type filter design

CHEN YEONG-CHIN

Department of Computer Science & Information Engineering, Asia University, 500 Liufeng Rd.,
Wufeng, Taichung 41354, Taiwan

In this paper, PSPICE is implemented to model and simulate the characteristic of thin film bulk acoustic resonator (FBAR). Both analogy equivalent circuits of Acoustic transmission line and Mason model is proposed and transferred to the PSPICE model by using the controlled-source method. The physical parameters such as piezoelectric materials and its thickness, electrode material, area and its thickness affecting the properties of the FBAS are discussed. Finally, we have implemented the FBAR to design a ladder type filter with a center frequency at 1.1 GHz and bandwidth about 60.9%. The study results in that PSPICE is an effective tool for the FBAR modeling and ladder type filter design.

(Received October 18, 2009; accepted September 15, 2010)

Keywords: Thin Film Bulk Acoustic Wave Resonator, FBAR, Resonator, Filter, PSPICE

1. Introduction

Mobile phones are one of the major driving forces for advancement in miniature electronics. New types of advanced wireless transceivers are entering the commercial market to meet the requirement of voice, data, and multimedia communications. With the development of very large scale integration (VLSI) and digital technology, tremendous improvement has taken place in the miniaturization of wireless communication subsystems. However there seems to be little room for improvement in the miniaturization of the established surface acoustic wave (SAW) and ceramic devices used for front-end RF filters, IF filters, and voltage –controlled oscillators (VCOs) since they are very difficult to fabricate on-chip. Thin-film bulk acoustic resonator (FBAR) technology represents a breakthrough in miniaturization of frequency-selective devices. Additionally, FBARs can be integrated directly onto the substrate of a semiconductor, resulting in a lower insertion loss and better handing capability [1, 2].

FBAR devices employ longitudinal thickness vibrations of the piezoelectric film to produce a resonant acoustic wave, and utilize the piezoelectric characteristics of the film to convert electrical energy into mechanical energy and vice versa. When an RF signal travels through the device, it expands and contracts in the form of mechanical vibrations of the entire piezoelectric layer. The piezoelectric transducer then excites the fundamental bulk compression wave, which travels perpendicularly to the film. A fundamental resonance condition is established when the thickness of the piezoelectric film is equal to an

integer multiple of a half of the wavelength of the input signal. Previous studies have reported that an FBAR must incorporate two acoustically reflective surfaces in order to trap energy and to produce the required resonator characteristics [3,4]. The response of the FBAR is similar to that of a simple bulk acoustic wave resonator. However, in the case of an FBAR, the piezoelectric layer is very thin (generally on the order of nm), and this enables the device to operate in the frequency range of 0.5 GHz to 10 GHz [3,4]. To optimize the design of an FBAR device, it is necessary to carefully consider the choice of material to be used for the piezoelectric film and for the top and bottom electrodes since the material properties not only determine the performance characteristics of the FBAR, but also influence the subsequent design of the FBAR filter. Hence, the present study investigates the relative influence of different piezoelectric film and electrode materials, and explores the impact of various physical parameters upon the performance of FBAR devices. Finally, the application of FBAR devices on ladder type filter design is discussed.

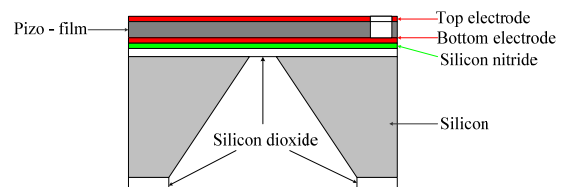


Fig. 1. Diagram of FBAR.

2. Equivalent circuit of FBAR

Fig. 1 depicts a schematic illustration of the four layered composite FBAR structure considered in the present study. It is observed that the device consists of: (1) a top electrode, (2) a piezoelectric film, (3) a bottom electrode, and (4) a membrane layer. Since it is necessary to prevent energy leakage during operation, the FBAR must be acoustically isolated from the substrate. Hence, a cavity is created beneath the resonant structure, and a membrane is usually performed using the one-dimensional mason model, in which the non-piezoelectric layers such as the electrodes and the membrane are treated as part of an acoustic transmission line [5].

The equivalent network of piezoelectric film can be represented by Mason [6] model as shown in Fig. 2. The parameters are defined as follows

$$Z_a = Z_b = jZ_0 \tan \frac{\kappa L_c}{2}, Z_c = -j \frac{Z_0}{\sin \kappa L_c}, \quad (1)$$

$$Z_0 = D_c V_c A_c, \kappa = \frac{\omega}{V_c}, \quad (2)$$

$$C_0 = \frac{A_c}{\beta_{33}^s L_c}, V_c = \left(\frac{C_{33}^D}{\rho} \right)^{\frac{1}{2}}, \quad (3)$$

and

$$N = C_0 h_{33} \quad (4)$$

where Z_a, Z_c is mechanical impedance, L_c is length of the film, Z_0 is acoustical characteristic impedance of piezoelectric film, D_c is density of ceramic, V_c is longitudinal velocity of propagation, A_c is cross-sectional area of ceramic, κ is longitudinal wave number, ω is angular frequency, V is electrical potential applied to the device, R_0 is dielectric loss resistance, C_0 is longitudinally clamped capacitance, N is electromechanical transformation ratio, β_{33}^s is dielectric impermeability, C_{33}^D is elastic stiffness, h_{33} is piezoelectric coefficient. The Mason equivalent circuit of the four layered composite FBAR shown in Fig. 1 is shown in Fig. 3 [7].

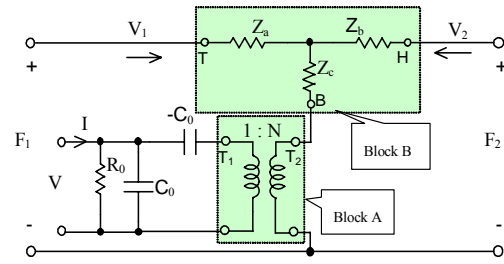


Fig. 2. Mason circuit of piezoelectric film vibrating in thickness mode.

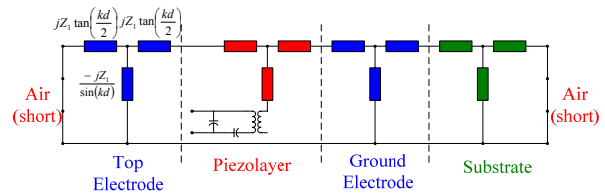


Fig. 3. Mason equivalent circuit of FBAR.

3. PSPICE Model of FBAR

Since a great deal of mathematical deduction of the effective compliance was required to estimate characteristics of FBAR, an analogous circuit and PSPICE model for the FBAR was proposed to facilitate the analysis of the frequency response and filter design. The PSPICE model of the analogous circuit of FBAR is described in detail as follows.

3.1 Electromechanical transformation circuit

Since the electromechanical transformation circuit, shown in block A of Fig. 2, is a transformer of electrical voltage and mechanical force, we modeled the circuit using the controlled source [8] method. The PSPICE model is expressed in Fig. 4 and the PSPICE code as given below.

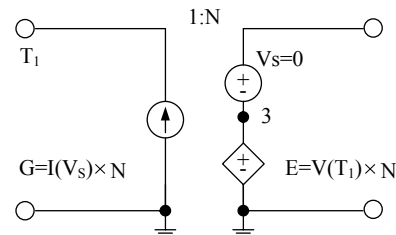


Fig. 4. PSPICE model of electromechanical transformation circuit.

**** PSPICE Model of Electromechanical Transformation circuit ****

```
.SUBCKT XTRANS T1 T2 PARAMS : N={0.94}
G 0 T1 VALUE = {I(VS)*N}
VS T2 3 DC 0
E 3 0 VALUE={V(T1)*N}
.ENDS
*****
```

3.2 Acoustical Transmission Line Model for the Passive film

The mechanical impedance of the piezoelectric film and the passive film such as top electrode, bottom electrode and membrane (silicon nitride) are modeled as acoustical transmission formation [9,10], shown in block B of Fig. 2. The impedance formula in the acoustical transmission formation model are transferred to a Laplace format by using the controlled source method [11,12] as shown in Fig. 5. Where the Laplace format of the impedance Z_a is

$$L\{Z_a\} = \frac{Z_a}{j\omega} S = jZ_0 \tan \frac{\kappa L_c}{2} \cdot \frac{S}{j\omega} = Z_0 \tan \frac{\kappa L_c}{2} \cdot \frac{S}{\omega} \quad (5)$$

Applying $\omega = (-S^2)^{\frac{1}{2}}$ and $\kappa = \frac{\omega}{v_a}$,

$$L\{Z_a\} = \frac{Z_m \cdot \tan\left(\frac{(-S^2)^{\frac{1}{2}} \cdot L_h}{2 \cdot v_a}\right) \cdot S}{(-S^2)^{\frac{1}{2}}} \quad (6)$$

and similarly,

$$L\{Z_b\} = \frac{Z_m \cdot \tan\left(\frac{(-S^2)^{\frac{1}{2}} \cdot L_h}{2 \cdot v_a}\right) \cdot S}{(-S^2)^{\frac{1}{2}}} \quad (7)$$

** PSPICE Model of Acoustical Transmission Line Model for the Passive film **

```
.SUBCKT XT_net B T H PARAMS: D={8.9E3} A={π*(20E-3)2} Va={3.5E3} Lt={45E-3}
.PARAM Zm={D*Va*A}
RCm B 2 1E-6
VCm 2 3 DC 0
Ecm 3 4 LAPLACE {I(Vcm)}={SQRT(-S*S)*Zm/(S*SIN(SQRT(-+S*S)*Lt/Va))}
RLt 4 5 1E-6
VLt 5 6 DC 0
Elt 6 T LAPLACE {I(VLt)}={Zm*S/(SQRT(-S*S)*
+ SIN(SQRT(-S*S)*Lt/Va))*(1-(M*COS(SQRT(-S*S)*Lt/Va))}
RLh 4 7 1E-6
VLh 7 8 DC 0
Elh 8 H LAPLACE {I(VLh)}={Zm*S/(SQRT(-S*S)*M*
+ SIN(SQRT(-S*S)*Lt/Va))*(1-(COS(SQRT(-S*S)*Lt/Va))}
.ENDS
```

3.3 PSPICE Model of Mason Circuit

The Mason circuit in Fig. 2 is described by electrical and mechanical portions linked with a transformer to convert the electrical voltage and mechanical force. The capacitance (C_o and $-C_o$) are described by frequency-

$$L\{Z_c\} = \frac{(-S^2)^{\frac{1}{2}} \cdot Z_m}{S \cdot \sin\left(\frac{(-S^2)^{\frac{1}{2}} \cdot L_h}{v_a}\right)} \quad (8)$$

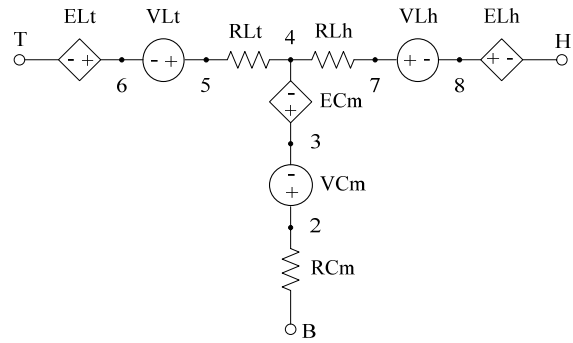


Fig. 5. PSPICE model of acoustical transmission.

The PSPICE code of acoustical transmission line is represented as follows.

domain device models of analog behavior modeling [13]. The subcircuits of the transformer (SUBCKT XTRANS) and mechanical T network (SUBCKT XT_net) are expressed as X_1 and X_2 in this PSPICE model, as follows.

```

***** ** * PSPICE Model of Mason Circuit ***** ** *
.SUBCKT XMA E MT MH PARAMS : C0={790E-12 }
R0 E 0 1E9
VC0 E 2 DC 0
RC0 2 3 1E-6
EC0 3 0 LAPLACE {I(VC0)} = {1/(1*S*C0)}
RC1 E 4 1E-6
VC1 4 5 DC 0
EC1 5 6 LAPLACE {I(VC1)} = {-1/(1*S*C0)}
X1 6 7 XTRANS PARAMS : N={N}
X2 7 MT MH XT_net PARAMS : D={Dc} A={Ac} Va={Vc} Lt={Lc}
.ENDS
    
```

4. Ladder type FBAR Filter

The building block for a single stage ladder filter consists of a series and shunt resonator, as shown in Fig. 6. The shunt resonator is designed to have a resonant frequency slightly lower than that of the series one, and its anti-resonance frequency is aligned with the resonance frequency of series element and the anti-resonance frequency of shunt element determine the pass-band of the filter; the anti-resonance frequency of series element and the resonance frequency of shunt element are the two transmission zeroes of filter. The stop-band rejection is determined by the impedance ratio, or static capacitor ratio, between the series and shunt element. A single ladder section gives a steep roll-off at pass-band edges, but a poor stop-band rejection. The method to improve stop-band rejection is to enlarge the static capacitor ratio, that is the

term $\frac{Z_s}{Z_p}$ FBAR, or cascade several ladder sections, but it will lead to large areas and increase the insertion loss.

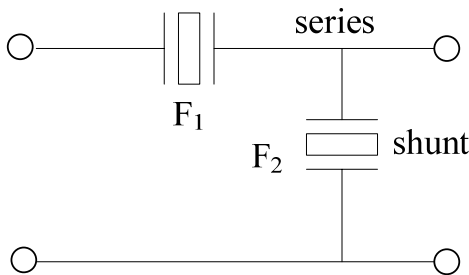


Fig. 6. Single stage Ladder-Type Filter.

5. Results and discussions

5.1 FBAR characteristics

The PSPICE model of FBAR is implemented to simulate the characteristics in all its aspects. Considering a FBAR device with a schematic as Fig. 1, ZnO is chosen to be the piezoelectric film of the FBAR with a thickness $T_{ZnO}=0.5\mu m$, aluminum is chosen to be the top and bottom

electrode with the same thickness $T_{Al}=0.18\mu m$, and the thickness of Silicon-Nitride is $T_{Si_3N_4}=0.2\mu m$. ZnO possesses a piezoelectric parameter $h_{33}=4.05E9$, electromechanical coupling factor $k_t=0.28$ and dielectric constant $\epsilon_r=8.8$. The properties of the materials are listed in Table 1.

Table 1. Properties of the FBAR's materials.

Name of materials	Sound velocity in the material (m/s)	Density(kg/m ³)
Zinc Oxide (ZnO)	$V_{ZnO} = 6340$ (m/s)	$\rho_{ZnO} = 5680$ (kg/m ³)
Aluminum (Al)	$V_{Al} = 6350$ (m/s)	$\rho_{Al} = 2695$ (kg/m ³)
Silicon Nitride (Si_3N_4)	$V_{Si_3N_4} = 6350$ (m/s)	$\rho_{Si_3N_4} = 2695$ (kg/m ³)

The impedance diagram of the FBAR with $T_{ZnO}=0.5\mu m$ is shown in Fig. 7, where the resonance frequency (f_s) is 3.3441GHz located at the point of minimum impedance, and the anti-resonance frequency (f_p) is 3.4085 GHz located at the point of maximum impedance.

When the piezoelectric films are varied in the thicknesses of 0.5 μm , 0.7 μm , 0.9 μm and 1 μm , the resonance frequency (shown in Fig. 8) are 3.3441 GHz, 8577 GHz, 2.4634 GHz and 2.1488GHz, individually. The resonance frequency increases as the thicknesses of piezoelectric film decreases, and the simulation results is similar to the experiment results of Kok Wan T and et al [14,15].

As we know, the resonance frequency (f_s) of the FBAR is attributed to thickness and sound velocity of the piezo-film, but how the electromechanical factor (K_t) of the piezo-film influences the characteristic of the FBAR? If we assume the properties of the piezo-film is the same except that the electromechanical factor is different and the simulation result in Fig. 9 reveals that the larger electromechanical factor ($K_t = 0.28, 0.38, 0.48$) it has the smaller resonance frequency ($f_s = 3.3441GHz, 3.2827GHz, 3.1937GHz$) is shown but the anti-resonance frequencies ($f_p = 3.4085GHz$) stay unchanged. This result also

concludes that larger electromechanical factor will improve the quality factor but degraded the bandwidth of the FBAR.

frequency ($f_p=3.4085\text{GHz}$) is independent of the area of the piezo-film.

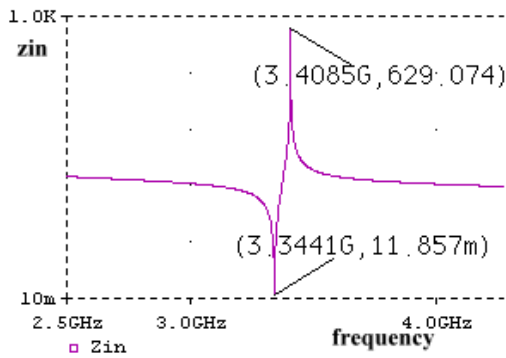


Fig. 7. The magnitude of FBAR impedance.

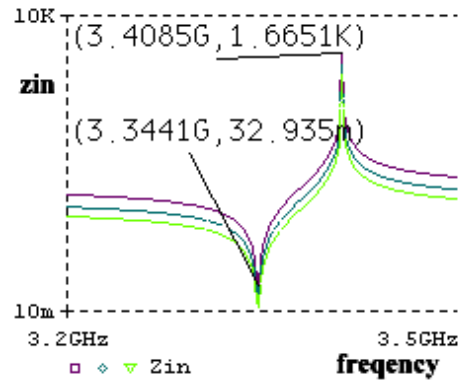


Fig. 10. Impedances of FBAR with different electromechanical factors.

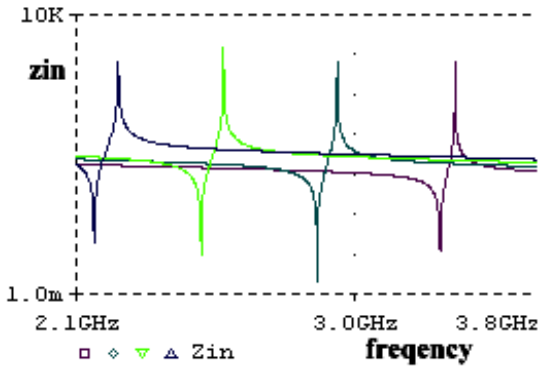


Fig. 8. The magnitude of FBAR impedance versus frequency with different thickness of piezo-film.

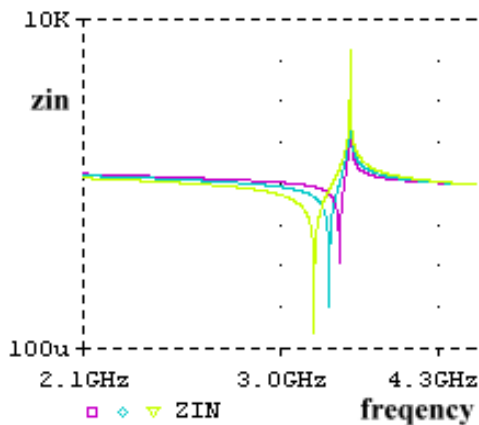


Fig. 9. The magnitude of FBAR impedance versus frequency with different electromechanical factors.

As the area of the piezo-film is set to $300(\mu\text{m})$, $400(\mu\text{m})$ or $500(\mu\text{m})$ separately, Fig. 10 shows that the resonance frequency ($f_s=3.3441\text{GHz}$) and anti-resonance

5.2 FBAR filter design

For a two stage ladder-type filter, the impedance of the series element and shunt element of the unity filter are respectively $Z_s=R_s+jX_s$ and $Z_p=R_p+jX_p$. To improve the stop-band rejection, the impedance (Z_s) of series element is chosen to be larger than that (Z_p) of shunt. In our study, the thickness of piezo-film of series FBAR is $1.87\mu\text{m}$, the thickness of piezo-film of shunt FBAR is $2.2\mu\text{m}$, the areas of the series element and shunt element of the FBAR are respectively $265(\mu\text{m})^2$ and $350(\mu\text{m})^2$, the thickness of upper and bottom electrode is $T_{Al}=0.01\mu\text{m}$ and the thickness of silicon-nitride $T_{Si_3N_4}=0.25\mu\text{m}$. Fig. 11 is the impedance magnitude of series FBAR, Fig. 12 is the impedance of shunt FBAR and Fig 13 is the transmission transform function of the two stage FBAR filter demonstrating a center frequency at 1.41GHz and bandwidth of 283MHz ($Bw\%=21.5\%$).

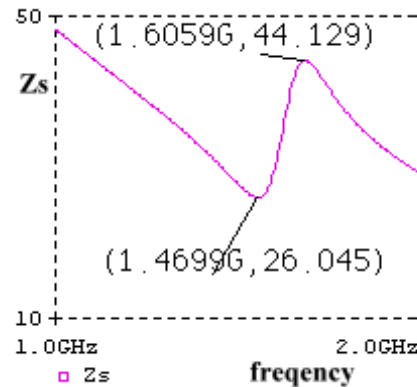


Fig. 11. The magnitude of series FBAR impedance versus frequency.

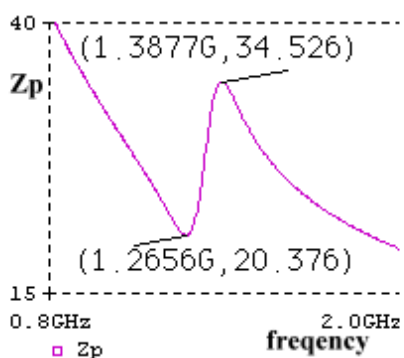


Fig. 12. The magnitude of shunt FBAR impedance versus frequency.

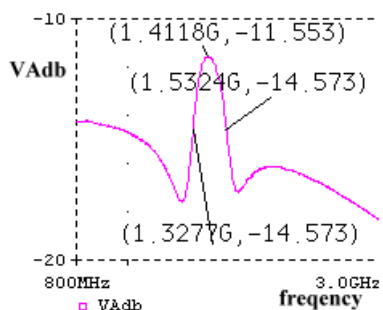


Fig. 13. The transmission transform function (TTF) of single stage ladder-type filter.

When the area of series and shunt FBAR is kept the same, the thicknesses of piezo-film of the shunt FBAR respectively vary as 1.87 μm , 2.4 μm , 3.0 μm , 3.6 μm , 4.2 μm and 4.8 μm , Fig. 14 shows that the 3.6 μm - thickness piezo-film of shunt FBAR will result in a larger bandwidth of (Bw%=60.9%).

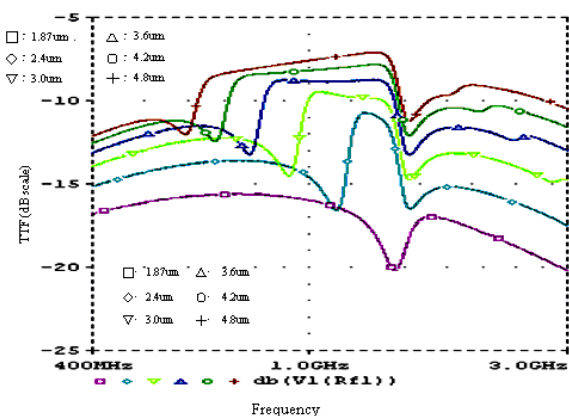


Fig. 14. The transmission transform function of two stages ladder-type filter by varying the piezo-film thickness as 2.2 μm , 2.8 μm , 3.6 μm , 4.6 μm , 5.8 μm and 6.8 μm , respectively.

The result is that the thicknesses of series FBAR is $T_{zno}=1.87\mu\text{m}$ and shunt FBAR is $T_{zno}=3.6\mu\text{m}$ will give a optimum wide band filter. If the area of series FBAR is $(265\mu\text{m})^2$, the area of shunt FBAR respectively vary as $(265\mu\text{m})^2$, $(285\mu\text{m})^2$, $(305\mu\text{m})^2$, $(325\mu\text{m})^2$, $(345\mu\text{m})^2$ and $(365\mu\text{m})^2$, Fig. 15 shows that the larger the area of shunt FBAR will give a higher stop-band rejection, but the bandwidth is still unchanged.

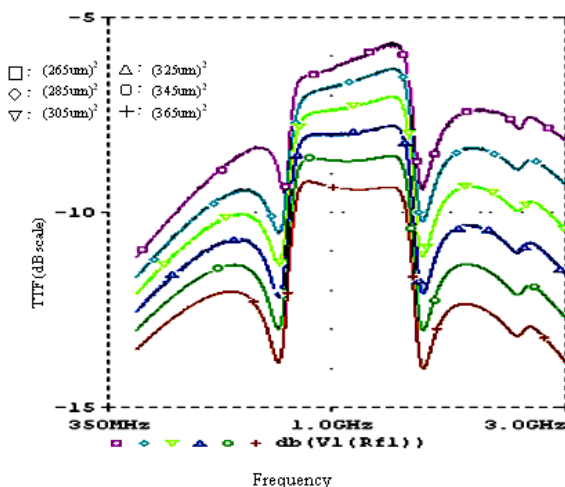


Fig. 15. The transmission transform function of two stages ladder-type filter by varying the piezo-film thickness as $(265\mu\text{m})^2$, $(285\mu\text{m})^2$, $(305\mu\text{m})^2$, $(325\mu\text{m})^2$, $(345\mu\text{m})^2$ and $(365\mu\text{m})^2$, respectively.

6. Conclusions

PSPICE model of FBAR is developed to study the characteristic depend on structure parameter and piezo-film properties. The simulation results are consistent with the theoretical deduction and experimental results. Some errors between simulation and measurement is due to the parameters definition of the model. The mason model does not model the transmission loss is one of the key issue of simulation discrepancy.

The PSPICE model of FBAR is implemented to design the ladder-type filter successfully. And found that this software is flexible for implementation on parameters optimization design. Factors such as device dimension, piezo-film thickness and electromechanical coupling factor that affects the characteristics of the filter are discussed and verified. The wide bandwidth FBAR filter is developed with a center frequency at 1.1GHz and bandwidth of 60.9%.

Acknowledgment

This work was supported by the National Science Council of the Republic of China under contract NSC 98-2221-E-468-023-

References

- [1] R. C. Ruby, P. Bradley, Y. Oshmyansky, A. Chien, III, J. D. Larson, IEEE Ultrasonics Symposium **1**(7-10), 813 (2001).
- [2] J. D. Larson, III, R. C. Ruby, P. D. Bradley, J. Wen, Shong-Lam Kok and A. Chien, IEEE Ultrasonics Symposium, **1**(22-25), 869 (2000).
- [3] M. Schmid, E. Benes, W. Burge, V. Kravchenko: Schmid, M. Benes, E. Burger, W. Kravchenko, V., IEEE Trans. Ultrason., Ferroelect., Freq. Contr. **38**, 199 (1991).
- [4] S. Horwitz, C. Milton, S. Horwitz, C. Milton, IEEE MTT-S Dig. **1**(1-5), 165 (1992).
- [5] K. M. Lakin, K. MIEEE, MTT-S Int. Microwave Symp. Dig. **1**(1-5), 149 (1992).
- [6] T. Inoue, T. Sasak, T. Miyama, K. Sugiuchi, S Takahashi, Trans. Inst. Electron. Inf. Commun. Engrs., **E70**, 909 (1987).
- [7] J. F. Rosenbaum, Bulk Acoustic Wave Theory and Devices, Artech House, 1988.
- [8] W. M. Leach, Jr., IEEE Trans. Ultrason. Ferroelectr. Freq. Control., **41**, (60), (1994).
- [9] W. Marshall Leach, Jr., IEEE Trans. on Ultrasonics, Ferroelectrics, and Frequency Control, **41**(1), 60 (1994).
- [10] G. Hayward, M. N. Jackson, IEEE Trans. Sonics and Ultrasonics, **SU-31**(3), 137 (1984).
- [11] P. W. Tuinenga, SPICE: A Guide to Circuit Simulation and Analysis Using PSPICE, 2nd ed. (Prentice-Hall, Englewood Cliffs, 1992).
- [12] The Design Center-Application Notes Manual, Version 6.1 (Microsim Corporation, Irvine, 1994), Chap. 1, p. 45.
- [13] Microsim PSPICE A/D & Basics+- User's Guide, Version 6.3 (Microsim Corporation, Irvine, 1996), Chap. 6, p. 36.
- [14] T. Kok Wan, H. Cheng-Liang, W. Long, Jap. Journal of Applied Physics **43**(3), 1122 (2004).
- [15] Z. Su, P. Kirby, E. Komuro, M. Imura, Q. Zhang, R. Whatmore, IEEE Trans. on Microwave Theory and Techniques, **49**(4), 769 (2001).

*Corresponding author: ycchenster@gmail.com